Appl. Phys. A 78, 9–14 (2004)
DOI: 10.1007/s00339-003-2295-1

Applied Physics A
Materials Science & Processing

L. DONG
J. JIAO✉
C. PAN
D.W. TUGGLE

Effects of catalysts on the internal structures of carbon nanotubes and corresponding electron field-emission properties

Department of Physics, Portland State University, Portland, OR 97207-0751, USA

Received: 4 July 2003/Accepted: 9 July 2003
Published online: 2 September 2003 •

ABSTRACT Using a chemical vapor deposition (CVD) method, multi-walled carbon nanotubes with uniform diameters of approximately 10 nm were synthesized on silicon substrates by the decomposition of acetylene using Fe, Co and Ni as the catalysts. Catalyst effects on the internal structures of the carbon nanotubes were evident in the Fe, Co and Ni catalyzed nanotubes. Although these nanotubes demonstrated similar morphologies, due to the variety of internal structures, the nanotubes synthesized from different catalysts demonstrated various electron field-emission characteristics including turn-on field, threshold field and field enhancement factor. Compared with carbon nanotubes from Ni catalyst, nanotubes from Fe and Co with the same diameters have better field-emission properties. Graphite layers in nanotubes from Fe and Co are much straighter and more parallel to the tube axis with fewer defects. For instance, the turn-on field and threshold field for nanotubes from Ni are 5 V/μm and 9 V/μm, respectively. These electric fields are much higher than those for nanotubes from Fe, which are 0.35 V/μm and 2.8 V/μm, respectively. This could be due to the effect of catalysts on the work function of nanotubes, since the catalyst particle usually terminates the free end of the nanotube, and the influence of internal structure on electron transportation along the nanotube axis. Therefore, this study suggests that besides a small diameter, good graphitization (crystallization) is an important prerequisite for a good carbon nanotube emitter.

PACS 79.70.+q; 68.37.Lp; 81.07.De

1 Introduction

Since their discovery in 1991 [1], carbon nanotubes have been investigated as electron field emitters for applications in flat-panel displays and electron microscopes [2–6]. Various methods have been used to synthesize carbon nanotubes, e.g. arc discharge, laser ablation and chemical vapor deposition (CVD). Among these methods, CVD is an effective way to synthesize patterned thin films of multi-walled carbon nanotubes. Nanotube growth positions can be controlled by the locations of catalysts on the substrates [7–9]. The catalyst compositions usually consist of iron (Fe), cobalt (Co), or nickel (Ni). Many studies concerning the growth of carbon nanotubes using Fe, Co and Ni as the catalysts have been reported [10–12]. In those reports, carbon nanotubes demonstrated different morphologies and internal structures due to the variety of nanotube growth parameters and catalysts used during the CVD process. Also, many papers about electron field-emission properties of carbon nanotubes have been published in which carbon nanotubes demonstrated various field-emission characteristics such as turn-on field, threshold field and field enhancement factor [13, 14, 16]. However, there is no systematic study and comparison of electron field emission from carbon nanotubes prepared by different catalysts. Many reports have only attributed the field-emission performance of carbon nanotubes to their high aspect ratio (size effect). Aside from the size effect, there is still relatively little known about the other factors affecting the emission properties of carbon nanotubes. In this study, we employed a high-resolution transmission electron microscope (HRTEM), and systematically characterized the internal structures of multi-walled carbon nanotubes synthesized by different catalysts (Fe, Co and Ni) using a thermal CVD method. The use of different catalysts results in the formation of carbon nanotubes with various internal structures. Furthermore, using a field-emission probe system, we investigated the influence of the internal structures of carbon nanotubes on their field-emission characteristics, including turn-on field, threshold field and field enhancement factor. The investigation of the correlations between the internal structures of the carbon nanotubes and their electron field-emission properties is important to further improve the field-emission properties of nanotube emitters and to understand their field-emission mechanism.

2 Experimental

2.1 *Preparation of catalyst film*

In this study, carbon nanotubes were synthesized on silicon substrates coated with a film of Fe, Co or Ni catalyst, respectively. Each catalyst film was synthesized using a very similar procedure. To prepare a Co film, firstly, the silicon substrates were ultrasonically cleaned in acetone for 5 min, followed by extensive rinsing with deionized water. The silicon sub-

✉ Fax: 503/725-9525, E-mail: jiaoj@pdx.edu

strates were dried using flowing N_2 gas. Then, cobalt nitrate solution (1.0 M, 15 ml) was mixed with tetraethoxysilane (10 ml) and ethanol (10 ml) followed by magnetic stirring for 20 min. Four drops of hydrogen fluoride were then added, and the mixture was stirred for another 15 min. After this process, a pink solution was obtained. While continuously being stirred to avoid the formation of a gel, the solution was dropped onto the surface of a silicon substrate to form a film. The coated silicon was then dried overnight at room temperature to evaporate excess water and other solvents. After this, the silicon substrate coated with Co catalyst was ready to be placed into a CVD system for the growth of carbon nanotubes.

Fe or Ni films were prepared using the same procedure as for the Co film, but the cobalt nitrate aqueous solution (1.0 M, 15 ml) was substituted for aqueous solutions of ferric nitrate (1.5 M, 15 ml) or nickel nitrate (1.5 M, 15 ml), respectively. A similar sol–gel method has been reported for the formation of the Fe catalyst film by Pan et al. [17, 18]. In our experiments, we further developed this sol–gel method to form Co and Ni catalyst films on the silicon substrates. Also, a much shorter time (2.5 h, instead of the 15 h used in Pan's experiments) was taken to calcinate and activate the Fe catalysts. Moreover, carbon nanotubes were synthesized using different CVD parameters, which included gas flow rates, ratios of H_2 to C_2H_2, nanotube growth temperature and growth time. The detailed parameters are described in the following paragraph.

2.2 *Growth of carbon nanotubes*

The silicon substrates coated with Fe, Co or Ni catalysts were placed in a ceramic boat in the center of a quartz tube, which was inserted into a horizontal tube furnace. The chamber was then evacuated to 3×10^{-2} Torr. After that, the following three steps were taken to synthesize carbon nanotubes: (1) catalyst calcination at 450 °C for 2 h under the vacuum condition of 3×10^{-2} Torr; (2) catalyst activation at 500 °C and at 75 Torr H_2 for 30 min. The flow rate of H_2 was 385 sccm; (3) carbon nanotube growth at 700 °C and at 75 Torr of an admixture of H_2 and C_2H_2 for 30 min. The flow rates of H_2 and C_2H_2 were 385 sccm and 25 sccm, respectively. After the growth period, the reaction chamber was evacuated to 3×10^{-2} Torr and allowed to slowly cool. When the reactor reached room temperature, the chamber was vented and the samples were removed.

To study the effect of H_2 on the formation of carbon nanotubes and their corresponding emission properties, in some experiments, no H_2 was introduced during the growth of carbon nanotubes. This means the first two steps were kept the same as described above, but in step (3), no H_2 was introduced. In step (3), carbon nanotubes were formed at 700 °C and at 75 Torr of C_2H_2 for 30 min. The flow rate of C_2H_2 was 25 sccm.

2.3 *Characterization of carbon nanotubes*

A FEI Sirion field-emission scanning electron microscope (FESEM) was used to characterize the morphology of the carbon nanotubes, and an FEI Tecnai F-20 field-emission HRTEM, equipped with an energy-dispersive X-ray (EDX) spectrometer, was used to characterize the internal structures of the nanotubes and to analyze their elemental compositions. To prepare the HRTEM samples, the carbon nanotubes were carefully scraped from the surface of the silicon substrates, dispersed in an ethanol solution and ultrasonicated for 5 min. Several drops of suspension were then transferred onto the TEM sample grids.

2.4 *Experimental setting for the measurement of electron field emission*

Field-emission investigations were carried out in a field-emission probe system with the sample at room temperature. The system base pressure was 2×10^{-8} Torr. As shown in Fig. 1, the test system had a point-to-plane electrode geometry between a tungsten probe anode (tip radius approximately 50 μm) and the carbon nanotubes formed on the planar silicon substrate cathode. The tungsten probe was connected through an 83.3 MΩ resistor to a Keithley 485 picoammeter floating at a variable power supply potential for the emission I–V measurement. Using silver paste, the silicon substrate was attached to a movable stainless steel plate. Reported voltages were corrected for the drop across the series resistor. The grounded cathode plate was connected to a micromanipulator; thus, the distance between the two electrodes and the lateral position of the substrate with respect to the anode could be adjusted through operating the micromanipulator. In our experiments, the distance between the electrodes was adjusted from 150 μm to 300 μm, which was three to six times larger than the radius of the tungsten anode probe (50 μm). The distance was measured with an optical microscope.

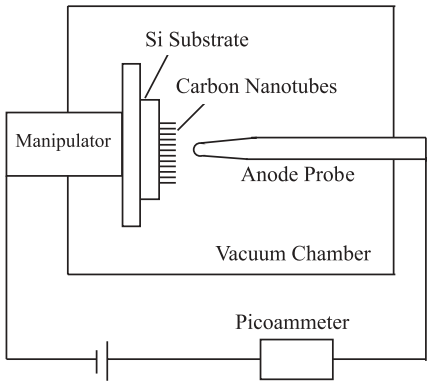

FIGURE 1 Schematic illustration of a field-emission probe system

3 Results and discussion

3.1 *Structural characterization*

SEM images in Fig. 2a and b show that the distribution of carbon nanotubes on the silicon substrate is related to the thickness of the catalyst films. When the thickness of the catalyst films was less than 1 μm, a thin film of carbon nanotubes was formed on the silicon substrate, as shown in Fig. 2a. When a large amount of catalyst solution was dropped onto the substrate surface, after the gel dried, the thick catalyst film cracked to form small pieces due to high surface tension. In this case the thickness of the catalyst film was about several μm to tens of μm. In the center regions of these catalyst pieces, aligned carbon nanotubes were formed perpendicular to the substrate, except for those nanotubes falling down on the edge (Fig. 2b). Our characterization suggests that the thicker the catalyst film, the higher the density of the nanotubes formed. A similar experimental

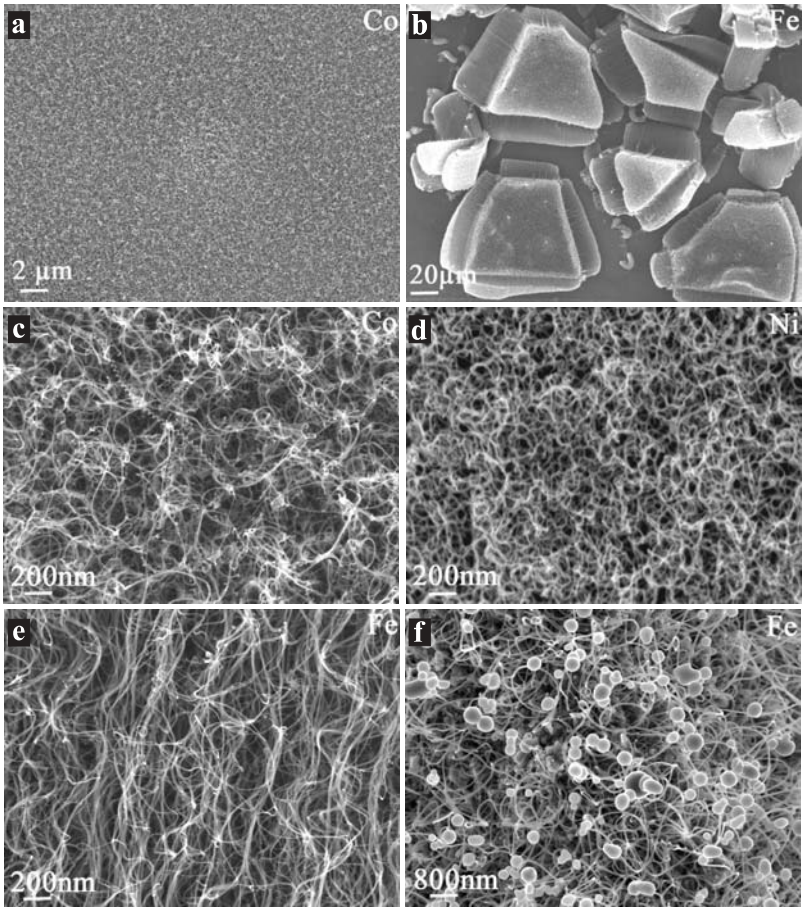

FIGURE 2 The configuration of nanotubes on the substrate is related to the thickness of the catalyst films. In **a**, a carbon nanotube film was formed on a thin catalyst layer. In **b**, a thick catalyst film has cracked to form separated catalyst regions. On the edge of each catalyst region, carbon nanotubes fall to the side, but the center parts are aligned perpendicular to the substrate. In **c**–**e**, SEM images of carbon nanotubes formed from Co, Ni and Fe catalysts, respectively, are shown. H_2 was introduced during these nanotube growths. In **f**, a SEM image of carbon nanotubes formed from Fe without H_2 introduced during nanotube growth is shown. The nanotubes obtained with larger diameters were mixed with amorphous carbon particles

result has been reported in [8]. SEM images in Fig. 2c–e were taken from nanotubes synthesized by decomposition of an admixture of H_2 and C_2H_2 using Co, Ni and Fe catalysts, respectively. A series of characterizations indicated that with the introduction of H_2 during nanotube growth, a high yield of high-purity carbon nanotubes with uniform diameters of 8–15 nm was synthesized on the silicon substrates. The length of the nanotubes ranged from 1 μm to 40 μm. There is no obvious diameter difference among the nanotubes from Co, Ni and Fe catalysts, but it is worth noting that nanotubes from Fe and Co were straighter than those nanotubes from Ni. Also, no particles were observed on the surface of the carbon nanotubes. This is because during nanotube growth at 700 °C, the introduction of a high ratio of H_2 to C_2H_2 (15 : 1 molar ratio) promotes the exothermic hydrogenation reaction of C_2H_2 to C_2H_6, which could increase the local temperature on the catalyst surface. The increased surface temperature then promotes the rapid decomposition of C_2H_6, which is the carbon source for forming the carbon nanotubes. This decomposition requires less energy than that required for the decomposition of C_2H_2 because the C–C bond of C_2H_6 (344 kJ/mole) is of much lower energy than the $C \equiv C$ bond of C_2H_2 (812 kJ/mole). Compared with the direct decomposition of C_2H_2 or C_2H_6, the proposed hydrogenation and decomposition process facilitates the formation of carbon nanotubes instead of carbon particles [19]. However, without involving H_2 in the growth process, the morphology of the products is different. Note that in Fig. 2f, using Fe as the catalyst but without H_2 introduced during nanotube growth, there are many particles formed on the surface of the carbon nanotubes, and the diameters of the nanotubes are larger than those in Fig. 2e (Note: the scale bar in Fig. 2e is 200 nm while in Fig. 2f it is 800 nm). The effect of H_2 on the formation of carbon nanotubes has been described in detail elsewhere [19]. The above experimental results suggest that there is no significant impact of different catalysts (Fe, Co or Ni) on the morphology of carbon nanotubes, except the nanotubes from Ni are more curved. However, the thickness of catalyst films and the introduction of H_2 during nanotube growth do influence the distribution and morphology of the carbon nanotubes.

In spite of the similar morphology of carbon nanotubes formed from Fe, Co and Ni, there are effects of the catalysts on the internal structures of the carbon nanotubes, such as the degree of graphitization and defects. As shown in Fig. 3a–c, nanotubes from Fe and Co catalysts have different internal structures to those from the Ni catalyst. For those nanotubes from Fe and Co (Fig. 3a and b), the graphite layers are straight and parallel to the tube axis (good graphitization). Nanotubes from Ni (Fig. 3c) have a similar diameter to those from Fe and Co, but these nanotubes have more defects and the graphite layers are not parallel to the tube axis. Our study also suggests that the introduction of H_2 during nanotube growth improves the graphitization of carbon nanotubes and decreases defects and diameter. As shown in Fig. 3a (with H_2 introduced) and Fig. 3d (without H_2 introduced), the average diameter of the nanotubes decreases from 45 nm to 12 nm, and the graphite layer becomes straighter with the introduction of H_2. Without H_2 introduction, graphitization only occurs inside nanotubes with a much thicker amorphous carbon outer layer, and moreover, the graphite layers are not straight and continuous.

As shown in the insets of Fig. 3a–d, catalyst particles of Fe, Co and Ni were observed to terminate the tips of the nanotubes, and were encapsulated within the carbon nanotubes. This suggests that Fe, Co and Ni particles lead the tip growth of carbon nanotubes [20].

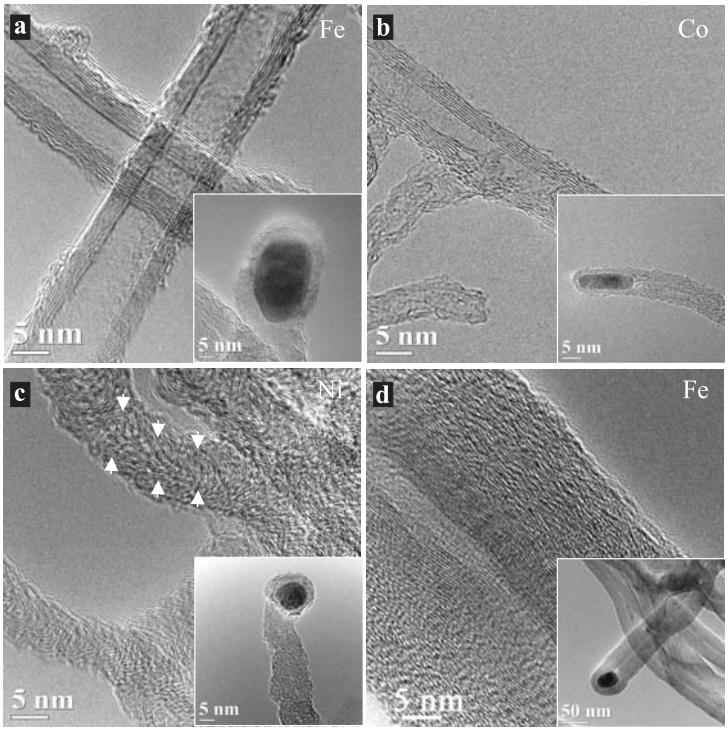

FIGURE 3 HRTEM images of carbon nanotubes synthesized from Fe, Co, and Ni, respectively **a–c**. HRTEM image of nanotubes from Fe without the introduction of H_2 during nanotube growth **d**. The *inserted images* in the *right bottom* of **a–d** show that catalyst particles were encapsulated within nanotubes

3.2 *Electron field-emission characteristics*

With regard to the electron field-emission of carbon nanotubes, many research reports have concluded that their emission performance is due mainly to the size effect. No systematic study concerning the effect of graphitization (or crystallization) of carbon nanotubes on their electron field-emission properties has been reported. Our measurements show that aside from the size effect, there is a graphitization effect on field emission (Fig. 4). The results are summarized in Table 1 (the turn-on fields and the threshold fields of the carbon nanotubes from Fe, Co and Ni). In general, the turn-on field and threshold field of a film emitter are defined as the macroscopic external field needed to extract a current density of 10 $\mu A/cm^2$ and 10 mA/cm^2, respectively. Current density J is defined as $J = I/\alpha$, where I is emission current (amperes) and α is the emission area of carbon nanotubes (cm^2). In our experiments, the emission area was considered as the tip area of the anode probe [21]. Since the same anode probe was used in all the field-emission measurements, the definition of emission area did not have an influence on the comparison study of turn-on fields and threshold fields of different nanotube emitters. Due to their similar morphologies and internal structures, both types of nanotubes obtained from Fe and Co catalysts had similar turn-on fields and threshold fields. As described above, there was no diameter size difference between nanotubes from Fe and Ni, but the turn-on field and threshold field of nanotubes from Ni were 5 V/μm and 9 V/μm, respectively. These electric fields are much higher than those for nanotubes from Fe, which are 0.35 V/μm and 2.8 V/μm, respectively. This is mainly because nanotubes from Ni do not have good graphitization. The explanation is discussed in detail later. Similarly, carbon nanotubes obtained from Fe catalyst without H_2 introduced, and thereby having a larger diameter and a low degree of graphitization, demonstrate much higher turn-on and threshold fields.

To further investigate the internal structure effects, we estimated the field-enhancement factor γ from the I–V characteristics and the corresponding Fowler–Nordheim (F–N) plots (Fig. 5). In different reports, the field-enhancement factor has been defined with different terms and assigned different symbols, e.g. field-amplification factor β [14] and field-enhancement factor β [22]. To avoid confusion with the historically defined local field factor β, we adopt the symbol γ for the field-enhancement factor [21, 23]. The field enhancement factor γ is defined as

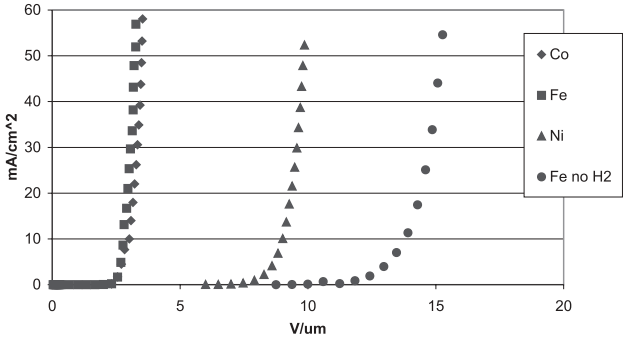

FIGURE 4 I–V characteristics of various carbon nanotubes synthesized from different catalysts

Type of nanotubes	Turn-on field (V/μm)	Threshold field (V/μm)	Enhancement factor
Nanotubes from Fe	~ 0.35	2.8	2300
Nanotubes from Co	~ 0.4	3	2600
Nanotubes from Ni	5	9	1500
Nanotubes from Fe without H_2	9.1	14	700

TABLE 1 Turn-on field, threshold field and enhancement factor for nanotubes from different catalysts (Fe, Co and Ni)

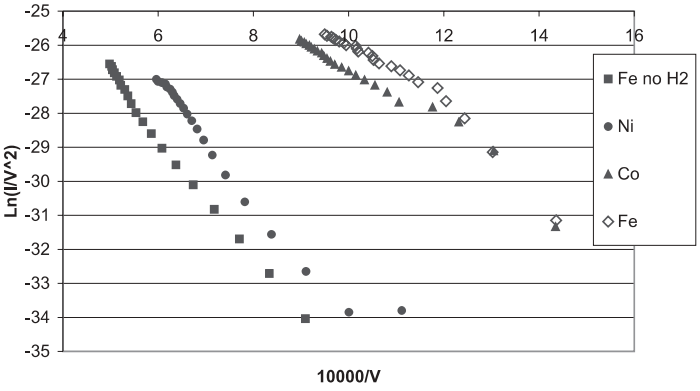

FIGURE 5 F–N plots of different carbon nanotubes, which correspond to the I–V characteristics in Fig. 4

$F = \gamma V/d$, where F is the local field on the surface of the nanotube tip, d is the distance measured between the two electrodes and V is the applied voltage. For a given work function, the factor γ is related to the geometrical shape of an emitter tip [14, 21, 23]. Due to a high curvature at the emitter tip, the local field is enhanced, and thus emission is increased. Based on the triangular-barrier approximation [23] and the F–N model [24], the slope S_{FN} of the F–N plot in Fig. 5 is given as follows:

$$\frac{\mathrm{d}\ln(J/F^2)}{\mathrm{d}(1/F)} = \frac{\gamma}{d}\frac{\mathrm{d}\ln(I/V^2)}{\mathrm{d}(1/V)} = \frac{\gamma}{d}S_{\mathrm{FN}} = -0.683\,\phi^{3/2} \tag{1}$$

Then, the factor γ can be calculated from the following equation:

$$\gamma = -0.683\frac{d}{S_{\mathrm{FN}}}\phi^{3/2} \tag{2}$$

In the above equations, ϕ is the work function of the nanotubes, which could vary from one nanotube to the next. Since the field-emission characteristics were measured from the films of carbon nanotubes instead of from an individual nanotube, in our calculations ϕ was assumed to be 5 eV [14]. According to the above assumptions and the slopes obtained of the F–N plots in Fig. 5, the field-enhancement factors γ for nanotubes from Fe, Co, and Ni with the introduction of H_2 are calculated to be 2300, 2600 and 1500, respectively. However, the factor γ for nanotubes synthesized from Fe catalysts without the introduction of H_2 is only about 700. Since emission currents were measured from many carbon nanotubes, the obtained factor γ here is a statistical average value. As we describe above, the factor γ depends only on the geometrical shape of the emitter, especially the radius of the emitter tip. Compared with nanotubes from Fe with the introduction of H_2 during nanotube growth, nanotubes from Fe but without the H_2 introduction have much larger diameters. Thus, they exhibit a small value of field-enhancement factor ($\gamma = 700$). However, with the introduction of H_2, nanotubes with similar diameters from Fe, Co, and Ni catalysts demonstrated a different value of factor γ. This is not consistent with the fact that with a given work function ϕ, the factor γ only depends on the radius of the emitter tip. This means we cannot simply assume that the nanotubes from Fe, Co and Ni have the same work function. Equation (2) clearly shows that the factor γ is not only related to the F–N slope S_{FN} but also the work function ϕ. As shown in the insets of Fig. 3a–c, the catalysts Fe, Co and Ni were encapsulated within the nanotube tips. The thickness of the outer graphite layers is about 1–5 nm. The existence of catalyst elements on the nanotube tips may have an effect on the work function ϕ of carbon nanotubes.

Besides the influence of diameter and work function, there could be other factors affecting the field-emission characteristics, such as the barrier to electron transportation along the nanotube axis. HRTEM results show that nanotubes from Ni have many defects. The internal graphite layers are not parallel to the nanotube axis. This type of internal structure may increase the resistivity to the electron transportation inside the nanotubes. A plausible explanation of the electron transportation along the nanotube axis is illustrated in Fig. 6. Compared with nanotubes from Fe and Co, there is a non-negligible resistance to the electron transportation inside of nanotubes from Ni due to the disordered internal graphite layers. This forms a resistance R that shares part of the external applied electrical potential. If the field-emission current obtained is I, the electric potential V' applied to the nanotube tip actually only equals V–IR. However, for the nanotubes from Fe and Co, V' equals V. This means that to obtain the same applied electric potential V', a higher electric potential V needs to be applied to the nanotubes from Ni. This could contribute to one of the reasons for the high turn-on field and threshold field for nanotubes from Ni. The obtained F–N plot slope and the inferred factor γ are therefore affected by the nanotube resistivity.

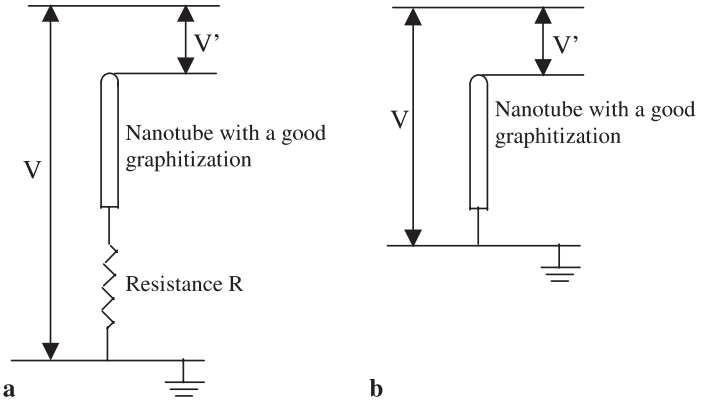

FIGURE 6 Schematic illustration of the resistance to electron transportation in nanotubes from Ni (**a**) and nanotubes from Fe and Co catalysts (**b**). The disordered graphite layers in the nanotubes from Ni increase the resistance to the electron transportation

4 Conclusions

In conclusion, multi-walled carbon nanotubes with a uniform diameter of approximately 10 nm were formed on silicon substrates by a thermal CVD method. A systematic electron microscopy study showed that nanotubes synthesized from different catalysts (Fe, Co and Ni) exhibit a similar morphology but have various internal structures, for example degree of graphitization and defects. Due to these different internal structures, the carbon nanotubes from Fe, Co and Ni have different electron field-emission properties, including turn-on field, threshold field and local enhancement factor. This suggests that besides the size effect, the degree of graphitization also has an impact on the field emission. Carbon nanotubes from Fe or Co demonstrate better field-emission properties than those from Ni.

ACKNOWLEDGEMENTS This research was financially supported by the National Science Foundation Grant Nos. DMR-0097575 and ECS-0217061, and the Donors of the American Chemical Society Petroleum Research Fund, Grant No. PRF-38108-G5.

REFERENCES

1 S. Iijima: Nature **354**, 56 (1991)
2 W.A. de Heer, A. Châtelain, D. Ugarte: Science **270**, 1179 (1995)
3 A.G. Rinzler, J.H. Hafner, P. Nikolaev, L. Lou, S.G. Kim, D. Tomanek, P. Nordlander, D.T. Colbert, R.E. Smalley: Science **269**, 1550 (1995)
4 W.B. Choi, D.S. Chung, J.H. Kang, H.Y. Kim, Y.W. Jin, I.T. Han, Y.H. Lee, J.E. Jung, N.S. Lee, G.S. Park, J.M. Kim: Appl. Phys. Lett. **75**, 3129 (1999)
5 N. Jonge, Y. Lamy, K. Schoots, T.H. Oosterkamp: Nature **420**, 393 (2002)
6 J. Jiao, L.F. Dong, D.W. Tuggle, C.L. Mosher, S. Foxley, J. Tawdekar: Mat. Res. Soc. Symp. Proc. **706**, 113 (2002)
7 S.S. Fan, M.G. Chapline, N.R. Franklin, T.W. Tombler, A.M. Cassell, H.J. Dai: Science **283**, 512 (1999)
8 L.F. Dong, J. Jiao, C.L. Mosher, S. Foxley: Mat. Res. Soc. Symp. Proc. **728**, 121 (2002)
9 J. Jiao, L.F. Dong, S. Foxley, C.L. Mosher, D.W. Tuggle: Microsc. Microanal. **9**, (2003)
10 J. Jiao, S. Seraphin: Chem. Phys. Lett. **249**, 92 (1996)
11 J. Jiao, P.E. Nolan, S. Seraphin, A.H. Cutler, D.C. Lynch: J. Electrochem. Soc. **143**, 932 (1996)
12 Z.P. Huang, D.Z. Wang, J.G. Wen, M. Sennett, H. Gibson, Z.F. Ren: Appl. Phys. A **74**, 387 (2002)
13 W. Zhu, C. Bower, O. Zhou, G. Kochanski, S. Jin: Appl. Phys. Lett. **75**, 873 (1999)
14 J.M. Bonard, J.P. Salvetat, T. Stöckli, L. Forró, A. Châtelain: Appl. Phys. A **69**, 245 (1999)
15 M. Sveningsson, R.E. Morjan, O.A. Nerushev, Y. Sato, J. Bäckström, E.E.B. Campbell, F. Rohmund: Appl. Phys. A **73**, 409 (2001)
16 M. Sveningsson, M. Jönsson, O.A. Nerushev, F. Rohmund, E.E.B. Campbell: Appl. Phys. Lett. **81**, 1095 (2002)
17 Z.W. Pan, S.S. Xie, B.H. Chang, L.F. Sun, W.Y. Zhou, G. Wang: Chem. Phys. Lett. **299**, 97 (1999)
18 Z.W. Pan, H.G. Zhu, Z.T. Zhang, H.J. Im, S. Dai, D.B. Beach, D.H. Lowndes: Chem. Phys. Lett. **371**, 433 (2003)
19 L.F. Dong, J. Jiao, S. Foxley, C.L. Mosher, D.W. Tuggle: J. Nanosci. Nanotech. **2**, 155 (2002)
20 S. Amelinckx, X.B. Zhang, D. Bernaerts, X.F. Zhang, V. Ivanov, J.B. Nagy: Science **265**, 635 (1994)
21 V.V. Zhirnov, C. Lizzul-Rinne, G.J. Wojak, R.C. Sanwald, J.J. Hren:J. Vac. Sci. Technol. B **19**, 87 (2001)
22 L. Nilsson, O. Groening, P. Groening, O. Kuettel, L. Schlapbach:J. Appl. Phys. **90**, 768 (2001)
23 A. Modinos: *Field, Thermionic and Secondary Electron Emission Spectroscopy* (Plenum Press, New York 1984)
24 R.H. Fowler, L.W. Nordheim: Proc. R. Soc. London Ser. A **119**, 173 (1928)